

Kinetic modeling of intense, short laser pulses propagating in tenuous plasmas

Patrick Mora

Centre de Physique Théorique (UPR 14 du CNRS), Ecole Polytechnique, 91128 Palaiseau, France

Thomas M. Antonsen, Jr.

Institute for Plasma Research and Departments of Electrical Engineering and Physics, University of Maryland, College Park, Maryland 20742

(Received 16 April 1996; accepted 14 October 1996)

Fast time averaged equations are derived for the motion of particles and the generation of electromagnetic wake fields under the action of the ponderomotive potential of an ultraintense laser pulse propagating through a tenuous plasma. Based on these averaged equations, a new particle code is designed which calculates the particle trajectories on the plasma period time scale. The regime of total cavitation of the plasma is investigated. It is found that stable propagation over a long distance is possible in this regime, and that energetic electrons are produced with a simple characteristic dependence of their angle of deflection on energy. This new code allows for computationally efficient modeling of pulse propagation over great distances. © 1997 American Institute of Physics. [S1070-664X(97)03301-6]

I. INTRODUCTION

Channeling of intense optical fields in plasmas is an important challenge, with possible applications in the context of laser plasma accelerators and x-ray lasers. Many nonlinear physical processes can be expected to affect the propagation of these intense pulses. In particular, it has been shown in recent papers that self-channeled intense laser pulses are subject to severe instabilities of the Raman type which modulate the laser pulse and erode its tail,¹⁻⁸ or cause the laser pulse to veer off its axis.^{9,10} The simulations and theory of Refs. 1-4 were based on laser-plasma fluid models corresponding to a cold plasma. This prevents one from treating situations where the plasma motion reaches the wave breaking limit and where fast electrons are generated in the interaction. In addition, these models contain a mathematical singularity at zero plasma electron density which prevents their use when the electrons are totally expelled from the axis of the laser propagation (electron cavitation). Such features are strong limitations of the fluid models in the high intensity regime. An alternative to the fluid models is the particle-in-cell (PIC) technique.^{7,8} This technique follows the evolution of the laser radiation on the short time scale associated with the laser period, and thus, is computationally intensive and restrictive in the parameters that can be studied.

In the following, a novel particle model is used to describe the long-time plasma behavior under the action of an ultrahigh intensity (of the order of 10^{18} W/cm² or more), short laser pulse (1 ps or less). Among the results we obtain, we emphasize the following: (i) Relativistic focusing for short laser pulses is possible over a long distance ($>30 z_R$) with total electron cavitation in the laser channel and strong reduction of the Raman type plasma instabilities ($z_R = \omega_0 r_L^2 / 2c$ is the Rayleigh length, ω_0 is the laser frequency, r_L is the laser spot size, and c is the light velocity). This self-focused propagation does not need the help of a preformed plasma channel,¹¹ which is necessary at moderate intensities. (ii) Plasma electrons can be ejected with relativistic

energies in the wake of the laser pulse. The angle of ejection is related simply to the electron energy as a consequence of momentum and energy conservation.

The organization of this paper is as follows. In Sec. II we will present our kinetic model and discuss the approximations used in its derivation. The actual detailed steps in the derivation are included in Appendix A. Properties of the model are also discussed in both Sec. II and Appendix B. Section III contains a discussion of the numerical implementation of the model for the case of a cylindrically symmetric laser envelope and plasma wake. Section IV contains some sample simulations illustrating the versatility of the code. Finally Sec. V contains our conclusions and a discussion of the direction of future work.

II. MODEL

The model we propose is fully relativistic, nonlinear, and kinetic.¹² In contrast to particle-in-cell techniques, however, approximations are made. Specifically, we make the following assumptions. Electrons interact with the radiation electric field in two separate ways. First, they jitter in response to the high frequency laser field, and thus contribute to a dielectric constant. Second, they respond to the low frequency ponderomotive potential of the laser field, creating a nonlinear wake following the laser pulse. This also modifies the dielectric constant through modification of the electron density and relativistic factor. Generally speaking, it is required that the plasma be tenuous for this separation of responses to be valid. In particular, we assume that the laser wavelength (frequency) is much smaller (greater) than all the other characteristic lengths (times) in the system. That is $\omega_p \ll \omega_0$ and $r_L \gg c/\omega_0$, where $\omega_p = (4\pi q^2 n_0/m)^{1/2}$ is the plasma frequency based on the ambient density n_0 , and $q = -e$ and m are the charge and mass of an electron. These inequalities enable one to expand the equation of motion of the electrons and the wave equation in powers of the small parameter ω_p/ω_0 .

A second approximation that we make with regard to the particle motion is the so-called quasistatic approximation (QSA),¹³ which assumes that the electron transit time through the laser pulse is short compared with the characteristic laser pulse deformation time. This approximation is valid for plasma electrons of sufficiently low energy. For these electrons, the laser pulse passes over quickly during which time its shape does not change. For electrons which have been accelerated to high energy, and which are traveling with the laser pulse, this approximation will fail. We made sure that in our simulations the number of electrons for which this is the case is zero or negligible.

Finally, consistent with our assumptions of a tenuous plasma, the plasma contribution to the dielectric constant will be small. Consequently, to lowest order the laser pulse will propagate without changing shape. Over a long distance and after a long time the shape of the pulse will evolve. This is treated in the envelope approximation. We will retain some higher order corrections to the envelope approximation, which allows the laser radiation to be considerably down-shifted in frequency. However, it is still assumed that the radiation is dominantly forward-propagating. Thus the development of backscattering instabilities is not treated in the present model.¹⁴ Due to the above approximations the relevant numerical time and space scales are the plasma period and the plasma wavelength, instead of the laser period and the laser wavelength as in PIC codes. This results in a considerable gain in terms of computing time. In addition, due to the separation of the electron response into high and low frequency components, we are able to treat the case of a cylindrically symmetric wake and an arbitrarily polarized laser pulse. It is believed that cylindrical effects are important in modeling the evolution of the head of the laser pulse which erodes due to diffraction.¹³

We begin our presentation with the envelope equation for the radiation. Here the radiation is written in terms of the high frequency vector potential $\hat{\mathbf{A}}_{\perp}$, which we write in the form of an envelope modulating a plane wave traveling at the speed of light,

$$\tilde{\mathbf{A}}_{\perp} = \hat{\mathbf{A}}_{\perp}(z, \mathbf{x}_{\perp}, t) \exp[ik_0 \zeta] + \text{c.c.}, \quad (1)$$

where k_0 is the wave number of the plane wave and $\zeta = z - ct$ measures the distance back from the head of the pulse. Here, the envelope, $\hat{\mathbf{A}}_{\perp}$, depends on time and space and is determined by

$$\left[\frac{2}{c} \frac{\partial}{\partial t} \left(ik_0 + \frac{\partial}{\partial \zeta} \right) + \nabla_{\perp}^2 \right] \hat{\mathbf{A}}_{\perp} = \frac{4\pi q^2}{mc^2} \left\langle \frac{\bar{n}}{\bar{\gamma}} \right\rangle \hat{\mathbf{A}}_{\perp}, \quad (2)$$

which follows from Eqs. (A32) and (A34). In writing the left-hand side of Eq. (2) we have dropped the term $\partial^2/\partial t^2$, which is of order $(\omega_p/\omega_0)^2$. In doing this we eliminate components of the radiation which appear to vary rapidly in the laser frame $\zeta = z - ct$. This corresponds to eliminating back-scattered radiation. Note that we have retained the mixed ζ - t derivative which is of order ω_p/ω_0 in our simulations. As discussed in Appendix B and shown in our numerical results, retention of this term allows one to model the absorption of radiation due to the creation of a plasma wake. Further, it can

be shown that inclusion of this term also enables one to model pure forward Raman scattering, which is normally excluded in the paraxial approximation.

The right-hand side of Eq. (2) represents the dielectric response of the plasma. The angular bracket represents an ensemble average over a distribution of particles each member of which has a slowly varying in time density, \bar{n} , and relativistic factor, $\bar{\gamma}$. In our numerical modeling this averaging will take the form of summing the contributions of the various simulation particles to the plasma dielectric.

The slowly varying density and relativistic factor are obtained by solving for the motion of a particle in the combined fields of the wake and the ponderomotive potential of the laser pulse. Specifically, the particles, in effect, satisfy the modified equation of motion,

$$\frac{d\bar{\mathbf{p}}}{dt} = q \left(\bar{\mathbf{E}} + \frac{\bar{\mathbf{v}}}{c} \times \bar{\mathbf{B}} \right) - \frac{q^2}{\bar{\gamma} m c^2} \nabla |\hat{\mathbf{A}}_{\perp}|^2, \quad (3)$$

where the overbar on each quantity signifies that it is slowly varying in time. Here the average relativistic factor is given by,

$$\bar{\gamma} = \sqrt{1 + \frac{1}{m^2 c^2} \left[|\bar{\mathbf{p}}|^2 + 2 \left| \frac{q}{c} \hat{\mathbf{A}}_{\perp} \right|^2 \right]}, \quad (4)$$

where the term under the radical involving the laser vector potential represents the contribution of the jitter motion of the electron to the transverse momentum. The derivation of Eqs. (3) and (4) for the specific case of interest is presented in Appendix A [see Eqs. (A21) and (A25)], where it is shown that their validity is limited to electrons for which $1 - v_z/c \gg \omega_p/\omega_0$ (in particular this excludes trapped particles from the range of validity of the model). We have also used the relation

$$\left| \frac{q}{c} \tilde{\mathbf{A}}_{\perp} \right|^2 = 2 \left| \frac{q}{c} \hat{\mathbf{A}}_{\perp} \right|^2,$$

which follows from averaging the square of expression (1) over the period of the laser.

The equations of motion (3) can alternatively be written in Hamiltonian form by introducing vector and scalar potentials $\bar{\mathbf{A}}$ and $\bar{\Phi}$ associated with the low frequency wake fields, and the canonical momentum $\bar{\mathbf{P}} = \bar{\mathbf{p}} + q\bar{\mathbf{A}}/c$. In this case the Hamiltonian is given by $\bar{H} = \bar{\gamma} m c^2 + q\bar{\Phi}$. In the quasistatic approximation, the Hamiltonian depends on z and t only in the combination $\zeta = z - ct$. This leads to the constancy of $\bar{H} - c\bar{P}_z$ via

$$\frac{d\bar{H}}{dt} = \frac{\partial \bar{H}}{\partial t} = -c \frac{\partial \bar{H}}{\partial \zeta} = -c \frac{\partial \bar{H}}{\partial z} = c \frac{d\bar{P}_z}{dt}. \quad (5)$$

For electrons which are initially at rest this implies

$$\bar{\gamma} m c^2 + q\bar{\Phi} - c\bar{P}_z - q\bar{A}_z = m c^2. \quad (6)$$

Equation (6) along with Eq. (4) can be used to solve algebraically for the axial momentum of a particle considering the perpendicular momentum, and scalar and vector potentials as known. In particular, introducing the potential

$$\bar{\psi} = \bar{\Phi} - \bar{A}_z, \quad (7)$$

we find

$$\bar{\gamma} = \frac{1}{2(1 - q\bar{\psi}/(mc^2))} \left\{ 1 + \frac{1}{m^2 c^2} \left[|\bar{\mathbf{p}}_{\perp}|^2 + 2 \left| \frac{q}{c} \hat{\mathbf{A}}_{\perp} \right|^2 \right] + \left(1 - \frac{q\bar{\psi}}{mc^2} \right)^2 \right\}, \quad (8)$$

and

$$\bar{p}_z = \frac{mc}{2(1 - q\bar{\psi}/(mc^2))} \left\{ 1 + \frac{1}{m^2 c^2} \left[|\bar{\mathbf{p}}_{\perp}|^2 + 2 \left| \frac{q}{c} \bar{\mathbf{A}}_{\perp} \right|^2 \right] - \left(1 - \frac{q\bar{\psi}}{mc^2} \right)^2 \right\}. \quad (9)$$

Thus, in solving the equations of motion, only the perpendicular components of momentum for a particle need to be evolved. The axial component can be obtained using Eq. (9). Specifically, we imagine solving the equations of motion on a two-or three-dimensional grid. We introduce the coordinate $\xi = ct - z = -\zeta$ so that positive ξ measures distance back from the head of the pulse, or alternatively, time at a fixed axial position. The evolution of the transverse momentum of a plasma particle as the pulse passes over it is then given by

$$\frac{d\bar{\mathbf{p}}_{\perp}}{d\xi} = \frac{1}{c(1 - q\bar{\psi}/(mc^2))} \left[q\bar{\gamma} \left(\bar{\mathbf{E}} + \frac{\bar{\mathbf{v}}}{c} \times \bar{\mathbf{B}} \right)_{\perp} - \frac{q^2}{mc^2} \nabla_{\perp} |\hat{\mathbf{A}}_{\perp}|^2 \right], \quad (10)$$

where we have used

$$\frac{d\xi}{dt} = c - \bar{v}_z = \frac{c}{\bar{\gamma}} \left(1 - \frac{q\bar{\psi}}{mc^2} \right) \quad (11)$$

and Eq. (6) in replacing the derivative with respect to time with a derivative with respect to the laser frame coordinate ξ . This replacement is useful in numerical solution of the governing equations as it allows particle quantities to be defined on the same axial grid as the field quantities. The trajectory of a particle in the transverse plane is then written,

$$\frac{d\mathbf{x}_{\perp}}{d\xi} = \frac{\bar{\mathbf{p}}_{\perp}}{mc(1 - q\bar{\psi}/(mc^2))}. \quad (12)$$

Once the electron trajectories in the $(\mathbf{x}_{\perp}, \xi)$ space are determined, the wake current densities and the dielectric constant for the laser field can be evaluated. As the laser pulse passes over an electron it contributes to the local density according to the amount of time it spends in a particular axial region. The effective density of the particle is then given by

$$\bar{n}(\mathbf{x}_{\perp}, \xi) = \bar{n}_0(\mathbf{x}_{\perp 0}) \frac{c}{c - \bar{v}_z} = \bar{n}_0(\mathbf{x}_{\perp 0}) \frac{\bar{\gamma}}{(1 - q\bar{\psi}/(mc^2))}, \quad (13)$$

where $\bar{n}_0(\mathbf{x}_{\perp 0})$ is the plasma density of the electrons upstream from the pulse. The density, $\bar{n}(\mathbf{x}_{\perp}, \xi)$, can be assigned to the grid in the transverse plane using techniques developed for PIC codes. The electrical current density may also be assigned based on the same procedure using Eq. (13) in Eq. (A35).

We note, in the speed of light frame, all information must propagate from small values of $\xi = ct - z$ to large values. Accordingly we integrate Eqs. (10) and (11) starting from $\xi = 0$, the head of the pulse. We must also write the equations for the wake fields so that they may be integrated in ξ in the same direction. To do this we rewrite the axial and transverse components of Eq. (A37) introducing the potential $\bar{\psi}$ defined in Eq. (7),

$$\frac{4\pi}{c} \bar{\mathbf{j}}_{\perp} = \nabla_{\perp} \frac{\partial \bar{\psi}}{\partial \xi} + \nabla_{\perp} (\nabla_{\perp} \cdot \bar{\mathbf{A}}_{\perp}) - \nabla_{\perp}^2 \bar{\mathbf{A}}_{\perp} \quad (14)$$

and

$$\frac{4\pi}{c} \bar{j}_z = -\frac{\partial^2 \bar{\psi}}{\partial \xi^2} - \nabla_{\perp}^2 \bar{A}_z - \frac{\partial}{\partial \xi} (\nabla_{\perp} \cdot \bar{\mathbf{A}}_{\perp}). \quad (15)$$

Solution of Eqs. (14) and (15) along with the charge continuity implied by solution of the particle equations then guarantees that the Poisson equation (A36) is satisfied as well.

The two transverse components of Eq. (14) can also be thought of as equations for the transverse solenoidal and irrotational parts of the current density (the last two terms on the right have zero transverse divergence). For a given current density, Eq. (14) can be solved for $\partial \bar{\psi} / \partial \xi$ and $\bar{\mathbf{A}}_{\perp}$ once a gauge condition is specified. An obvious choice, which we make here is the transverse Coulomb gauge, $\nabla_{\perp} \cdot \bar{\mathbf{A}}_{\perp} = 0$. Then we have from Eq. (14)

$$\frac{4\pi}{c} \nabla_{\perp} \cdot \frac{\partial \bar{\mathbf{j}}_{\perp}}{\partial \xi} = \nabla_{\perp}^2 \Gamma, \quad (16)$$

where Γ is given by

$$\frac{\partial^2 \bar{\psi}}{\partial \xi^2} = \Gamma. \quad (17)$$

The left-hand side of Eq. (16) is determined from the particle equations, and Eq. (16) is inverted to find Γ . With Γ known, Eq. (17) may be integrated axially to determine the potential $\bar{\Psi}$, and Eqs. (14) and (15) (with $\nabla_{\perp} \cdot \bar{\mathbf{A}}_{\perp} = 0$) inverted to find $\bar{\mathbf{A}}$.

To summarize, within the stated assumptions, the determination of the plasma response to an intense laser pulse is as follows. Trajectories of individual particles are obtained by integrating Eqs. (10) and (11) forward in ξ . The axial momentum and relativistic factor for individual particles are determined from Eqs. (8) and (9). Simultaneously, one integrates Eqs. (16) and (17) to find the potential and then inverts the transverse Laplacians in Eqs. (14) and (15) to find $\bar{\mathbf{A}}_{\perp}$ and \bar{A}_z . Finally, one computes the plasma dielectric and integrates Eq. (2) in time to evolve the laser fields. The procedure is then repeated for a fresh group of plasma particles. The realization of this system for a cylindrically symmetric laser pulse will be discussed in Sec. III.

III. NUMERICAL REALIZATION

We have solved the set of Eqs. (6) and (19)–(22) on both a two-dimensional Cartesian grid (ξ, x) and a cylindrical grid (ξ, r_{\perp}) with the computer code WAKE. The numerical method is implicit as far as weakly nonlinear terms are concerned, and the remaining terms in the equations of motion are

treated using a predictor corrector scheme. Once the particle trajectories are computed, we collect the terms contributing to the right-hand side of Eq. (2) to advance the laser field in time with a time step which is a fraction of the Rayleigh length divided by the light velocity. Finally we also treat the ions' motion and contribution to the source in Maxwell equations. However, except for quite long laser pulses, when the ions tend to be expelled from the laser channel by the ambipolar field due to the electron expulsion, the simulation results are almost insensitive to whether or not the ions are allowed to move.

In the case of two-dimensional geometry the transverse Coulomb gauge condition implies $\mathbf{A}_\perp=0$. Further, we combine Eqs. (15) and (16) to form the modified equation

$$\frac{4\pi}{c} \left(\nabla_\perp \cdot \frac{\partial \bar{\mathbf{j}}_\perp}{\partial \xi} + k_p^2 \bar{j}_z \right) = (\nabla_\perp^2 - k_p^2) \Gamma - k_p^2 \nabla_\perp^2 \bar{A}_z, \quad (18)$$

where $k_p = \omega_p/c$, which is inverted to find Γ as opposed to Eq. (16). This equation has the feature that in the weakly nonlinear, electrostatic limit it produces the same equation as fluid theories for the excitation of the plasma wave.

Finally, to simplify matters we have introduced the following normalized quantities: $\mathbf{a}(r, t) = q\hat{\mathbf{A}}_\perp/mc^2$, $\mathbf{p} = \bar{\mathbf{p}}/mc$, $\psi = -q\bar{\psi}/mc^2$, $r = k_p r$, $\xi = k_p \xi$, and $\mathbf{b} = -q\nabla \times \mathbf{A}/m\omega_p c$. In cylindrical geometry this results in the following equation of motion:

$$\frac{dp_r}{d\xi} = \frac{1}{1+\psi} \left(\gamma \frac{\partial}{\partial r} \psi - \frac{1}{2} \frac{\partial}{\partial r} \langle a^2 \rangle \right) - b_\theta, \quad (19)$$

$$\frac{dr}{d\xi} = \frac{p_r}{1+\psi}, \quad (20)$$

and the following equations for the wake field;

$$(\Delta_\perp - 1) \frac{\partial^2}{\partial \xi^2} \psi = \frac{1}{r} \frac{\partial}{\partial r} r \left(\frac{\partial j_r}{\partial \xi} - b_\theta \right) + j_z, \quad (21)$$

$$\frac{1}{r} \frac{\partial}{\partial r} r b_\theta = \frac{\partial^2}{\partial \xi^2} \psi + j_z. \quad (22)$$

The equations are solved using a finite difference scheme in which a grid is set up in both axial coordinate ξ and radial coordinate r . Certain quantities are defined on the grid or halfway between two grids. For example, among the field quantities the radiation vector potential a , the normalized wake potential ψ and its second derivative Γ , the density \bar{n} and dielectric constant, and the axial current density j_z are all defined on both the radial and axial grid. The azimuthal magnetic field and radial electric field are defined on the axial grid and halfway between to radial grid points. The axial electric field is defined on the radial grid, but halfway between two axial grid points, and the radial current density is defined halfway between both the radial and axial grid points. For the particles, the radial location, relativistic factor, and axial velocity are calculated on the axial grid, whereas the radial momentum is defined halfway between two axial grid points.

The following radial boundary conditions are used. In inverting Eq. (21) it is assumed that the wake potential is regular at the origin and vanishes at a sufficiently large ra-

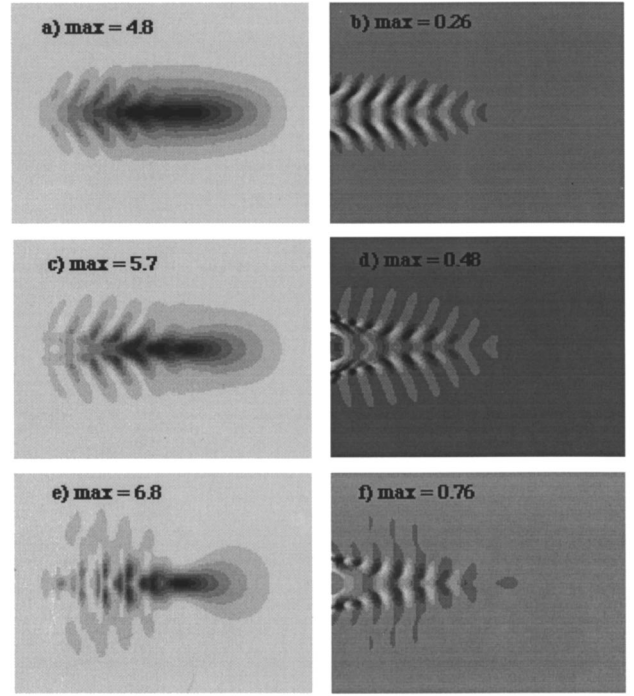


FIG. 1. Contour plots from a two-dimensional planar simulation with $a_0=0.375$, $\omega_0/\omega_p=5.0$, $k_p r_L=9$, and $k_p L=80$. The size of the simulation box shown are $85 k_p^{-1}$ along z and $63 k_p^{-1}$ in the perpendicular direction: (a) laser field and (b) axial wake electric field at $\omega_p t=100$, (c) laser field, and (d) axial wake electric field at $\omega_p t=150$, (e) laser field, and (f) axial wake electric field at $\omega_p t=250$.

dius corresponding to the boundary of the simulation volume. The azimuthal magnetic field is assumed to be regular at the origin. Concerning the particles, those which intersect the symmetry axis are specularly reflected. For the laser field Eq. (2) is solved subject to the outgoing radiation boundary condition discussed in Ref. 1. Numerical solutions of the above system of equations will be presented in Sec. IV.

IV. SAMPLE RESULTS

We verified that the code gives identical results to Ref. 1 (slab geometry) in the weakly relativistic limit and to Ref. 2 (cylindrical geometry) when the electron flow is laminar. We also compared the code with the results of a PIC code⁷ for values of ω_p/ω_0 as large as 0.2, and in situations where the QSA is only marginally valid, and the code gave very close results, with a lower noise in our case. Sample results from this latter case are shown in Fig. 1. The following parameters were chosen: $a_0=3/8$, $k_p r_L=9$, and $\omega_p/\omega_0=0.2$. The initial profile for the laser radiation was selected to be of the form,

$$a(r, \xi, t=0) = a_0 f(\xi) \exp(-r^2/r_L^2),$$

where $f(\xi)$ increases linearly from 0 to 1 for $0 < k_p \xi < 30$, $f(\xi)=1$ for $30 < k_p \xi < 50$, and $f(\xi)$ decreases linearly from 1 to 0 for $50 < k_p \xi < 80$. Figure 1 displays the gray scale plots of the amplitude of the laser electric field, and the axial low frequency wake electric field in the x, ξ plane at several different times. This figure can be compared with Fig. 3 of Ref. 7. One can see that the qualitative features of the evolution of the laser pulse are in good agreement, and that

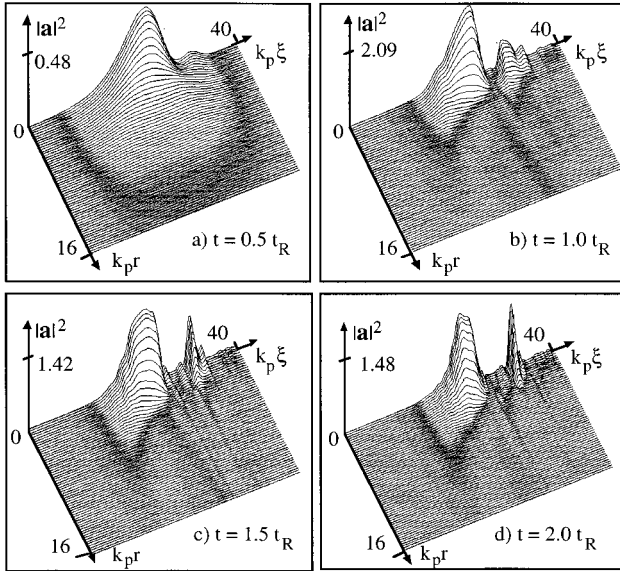


FIG. 2. Time evolution of the laser intensity for the case of a moderate intensity and large focal spot ($a_0=0.25$, $k_p r_L=16$, $k_p L=40$).

quantitatively there is reasonably good agreement as well, though trapped particles are seen in Ref. 7, while they are not treated in the present model.

We now show the result of a high intensity laser pulse propagating in a tenuous plasma in cylindrical geometry. Initially, the radiation is of the form

$$a(r, \xi, t=0) = a_0 \sin(\pi \xi / L) \exp(-r^2 / r_L^2).$$

The following parameters were chosen: $a_0=0.25$, $k_p L=40$, $k_p r_L=16$, and $\omega_p / \omega_0=0.03$, which corresponds to a plasma of density 10^{18} cm^{-3} for a $1 \mu\text{m}$ laser light. Figure 2 shows surface plots of the laser intensity at four times during the simulation. The power is about twice the critical power for relativistic self-focusing^{15,16} [$P_c = 16.2(\omega_0 / \omega_p)^2 10^9 \text{ W}$]. As expected, we observe that the pulse is subject to the Raman self-focusing instability.¹ However we observe that the instability develops slightly slower than predicted by the weakly nonlinear model of Ref. 1. After one Rayleigh length, we observe that the pulse has been separated into two pulses which are still focused and propagate on about 2 Rayleigh lengths, and then diffracts quickly after a strong pump depletion.⁸ The same case run with $\omega_p / \omega_0=0$, that is without the $\partial/\partial \xi$ term in Eq. (2), would propagate on about 10 Rayleigh lengths, which shows the importance of the pump depletion and of the forward Raman term here.

Figure 3 corresponds to the same laser power, but to a smaller focal spot, i.e., $a_0=1.0$, $k_p r_L=4$. In this case, we observe a total expulsion of the electrons from the laser channel which stabilizes the Raman instability in the bulk of the laser pulse. As a result, the laser pulse propagates over a large distance (more than 30 Rayleigh lengths) with a radial profile similar to the one predicted in the model of Sun *et al.*¹⁶ The front part of the pulse is eroded as predicted by Sprangle *et al.*¹³ The fact that self-focused propagation on distances much larger than the Rayleigh length is possible is in agreement with recent experimental results.^{17,18} We veri-

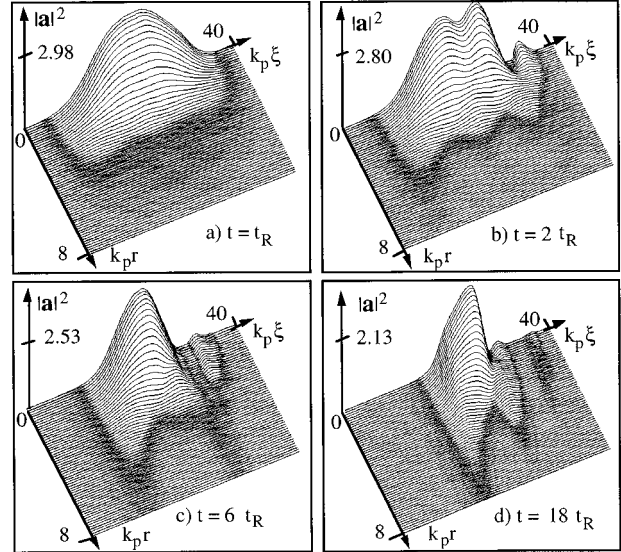


FIG. 3. Time evolution of the laser intensity for the case of a large intensity and small focal spot ($a_0=1.0$, $k_p r_L=4$, $k_p L=40$).

fied here that the role of the forward Raman term was apparently smaller in this case. Note however that as the Rayleigh length scales as r_L^2 , the actual distance on which the laser pulse propagates is not much different in the small focal spot case than in the case of Fig. 2.

Figure 4 shows the electron density after one Rayleigh length for the same case as Fig. 3. One observes total electron cavitation where the laser intensity is large, enhancement of the density on the sides of the self-focused channel, and a strong peak behind the laser pulse due to electrons which come back toward the center of the channel under the action of the charge separation field. This behavior is similar to that observed in the case of the nonlinear plasma wake field.¹⁹ Suppression of Raman instabilities may be attributed to a number of effects. The electron density is reduced where the laser intensity is greatest, the plasma channel is inhomogeneous which disturbs the plasma wave resonance, and the channel density has a maximum at a radius just greater than the spot size. This last effect contributes to enhancing the diffraction of radiation which is side scattered and thus suppresses side scattering instabilities.²⁰

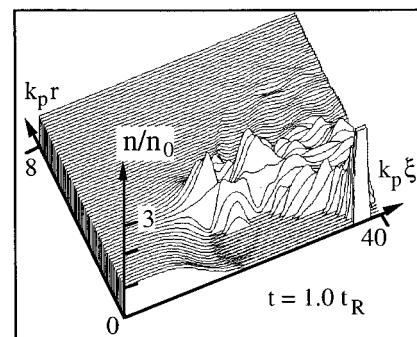


FIG. 4. Electron density after one Rayleigh length (same case as Fig. 3). The electron density has been limited to $3 n_0$ on this curve.

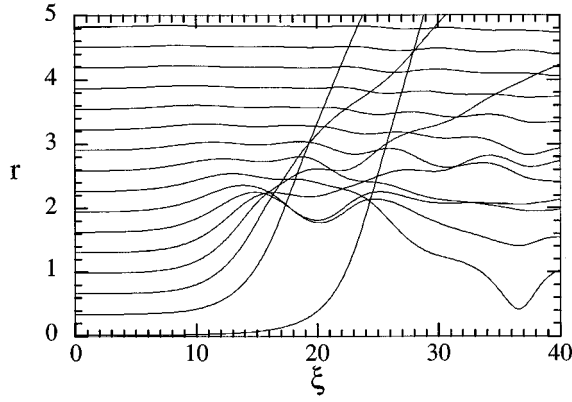


FIG. 5. Sample electron trajectories for the case of Figs. 3 and 4, after the laser pulse has propagated 1 Rayleigh length in the plasma.

Figure 5 shows sample electron trajectories after the laser has propagated one Rayleigh length in the plasma. In this example the electron flow is laminar until $k_p \xi \approx 15$. For $k_p \xi > 15$, the radial wavebreaking of the plasma disturbance results in a multi-peaked electron distribution function and the ejection of fast electrons in the MeV range. The validity of fluid codes would be limited to $k_p \xi < 15$ here. Figure 6 shows the cross section $\sigma(E)$ for the generation of electrons with energy greater than E . This cross section is generated after the laser pulse has propagated 30 Rayleigh lengths in the plasma. It is averaged over the propagation length and normalized to $\sigma_0 = 2\pi(c/\omega_p)^2$. The rate of production R of electrons with energy greater than E is given by

$$R = \sigma(E) n_0 c = 5.3 \times 10^{22} \frac{\sigma(E)}{\sigma_0} \text{ s}^{-1}. \quad (23)$$

In the example shown in Fig. 6, the maximum Lorentz factor of the accelerated electrons is of the order of 3, which is well below the validity limit of the ponderomotive approach [Eq. (3)], since here $\omega_0/\omega_p = 33$. Due to the constraint, Eq. (6), the ejected electrons (for which $\psi = 0$) satisfy the relation $p_z = \frac{1}{2} p_r^2$. Note that this relation applies to the electrons accelerated by the ponderomotive force (and self-consistent plasma fields), and that it has the same form as the relation between

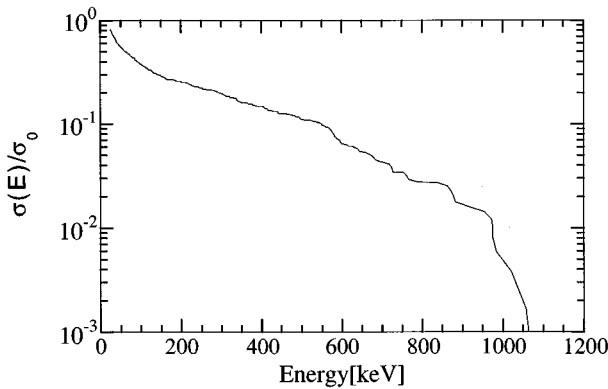


FIG. 6. Cross section for the generation of electrons with energy greater than E in the case of Figs. 3–5. The fast electrons are collected over the first 30 Rayleigh lengths.

the axial and the radial jitter momentum of an electron in a plane wave.²¹ It does not apply to longitudinally trapped electrons which violate the validity limit of the ponderomotive approach. The relation may be reexpressed in terms of the angle θ made by the electron with respect to the axis of the laser,

$$\cos \theta = \sqrt{\frac{\gamma - 1}{\gamma + 1}}. \quad (24)$$

A simple interpretation of this result can also be given by the analysis of the collision of a photon packet (of total energy $E \gg mc^2$) with a single electron when the energy loss of the radiation is small (multiphoton Compton effect with small photons deflection). This relation can be expected to apply so long as the radiation wave vector remains in the forward direction. Electrons satisfying this relation were recently observed by Meyerhofer *et al.* in a laser-gas experiment.²²

A final set of simulations correspond to cases typical of contemporary experiments.¹⁸ The parameters of the reference run for this set are $a_0 = 1.083$, $k_p r_L = 3.713$, $\omega_p/\omega_0 = 0.0594$, which correspond to $1.058 \mu\text{m}$ laser light, $r_L = 10.54 \mu\text{m}$, $z_R = 330 \mu\text{m}$, $n_0 = 3.5 \times 10^{18} \text{ cm}^{-3}$, $P = 10 \text{ TW}$, $P/P_c \approx 2.2$, and $I_0 = 5.73 \times 10^{18} \text{ W cm}^{-2}$ (where P is the laser power and I_0 is the maximum laser intensity when focused in vacuum). The plasma length is 3 mm long ($9 z_R$), including two linear ramps of one Rayleigh length on each side. The temporal pulse profile is Gaussian with a full width at half-maximum in energy of 300 fs ($\approx 31.7 \omega_p^{-1}$). The simulation box extends to $12 r_L$. In the reference run (curves A on Figs. 7 and 8) the laser is focused near the entrance of the gas jet, namely at $z/z_R = -3.5$, where $z = 0$ corresponds to the center of the gas jet. Figures 7 and 8 show the maximum intensity attained on the laser axis as a function of the position $z = ct$. Due to self-focusing the intensity grows up to approximately $3.5 I_0$, and the laser pulse then propagates in a self-focused state with $I/I_0 \approx 2-2.5$ until the exit of the jet. As in the case corresponding to Fig. 3, we have verified that the self-focused part of the pulse progressively shortens as the pulse propagates in the plasma, while there is a complete electron density cavitation with the formation of a strongly nonlinear wake. In the case of Figs. 7 and 8, we have varied some parameters compared to the reference case.

For the case of Fig. 7(a) we have varied the laser intensity. Curve B corresponds to $a_0 = 0.766$, or $I_0 = 2.86 \times 10^{18} \text{ W cm}^{-2}$, $P = 5 \text{ TW}$, $P/P_c \approx 1.1$. Though the laser power is still slightly above the critical power, it is not sufficient to maintain self-focused propagation over a long distance as in the reference case. Curve C corresponds to $a_0 = 0.01$ and shows no nonlinear effect. One recovers in this case the vacuum propagation characteristics.

For the case of Fig. 7(b) we have varied the electron density. Curve B corresponds to the same laser parameters as curve A except for the density which is $n_0 = 7 \times 10^{18} \text{ cm}^{-3}$, so that $P/P_c \approx 4.4$. One observes a similar behavior, with an even stronger amplification of the maximum laser intensity, which attains $4-6 I_0$, in a smaller density channel.

For the case of Fig. 7(c) we have varied the focal position, from near the entrance of the gas jet to near the exit of it. More specifically, the focal position (in vacuum or for

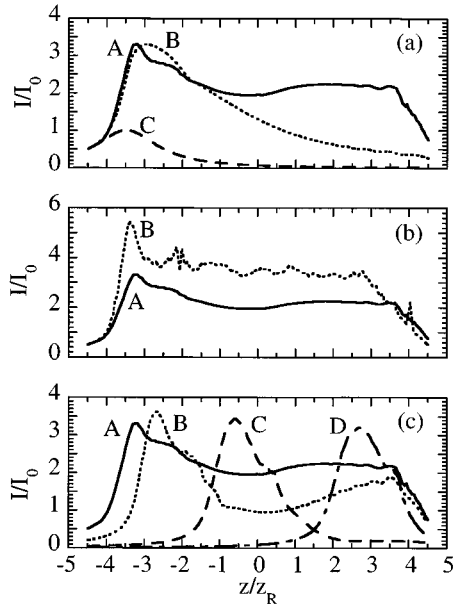


FIG. 7. On-axis maximum intensity (normalized to the maximum intensity when focused in vacuum) as function of the propagation distance. Curves A always correspond to the following physical parameters, $r_L=10.54 \mu\text{m}$, $z_R=330 \mu\text{m}$, $n_0=3.5 \times 10^{18} \text{ cm}^{-3}$, $P=10 \text{ TW}$ ($P/P_c \approx 2.2$), for a $1.058 \mu\text{m}$ laser light. The plasma length is 3 mm long ($9 z_R$), including two linear ramps of one Rayleigh length on each side. The temporal pulse profile is Gaussian with a full width at half-maximum in energy of 300 fs. The laser is focused near the entrance of the gas jet, namely at $z/z_R=-3.5$, where $z=0$ corresponds to the center of the gas jet. (a) Same parameters as curve A except for the laser intensity, $P=5 \text{ TW}$ (curve B), and $P=1 \text{ GW}$ (curve C); (b) same parameters as curve A except for the plasma density, $n_0=7 \times 10^{18} \text{ cm}^{-3}$ (curve B); (c) same parameters as curve A except for the focal spot position, $z/z_R=-2.5$ (curve B), $z/z_R=0$ (curve C), and $z/z_R=+3.5$ (curve D).

$a_0 \ll 1$) corresponds, respectively, to -3.5 (curve A), -2.5 (curve B), 0 (curve C), and $+3.5$ (curve D). The simulation box has been extended respectively to 16 and $20r_L$ for the cases corresponding to curves C and D, respectively. One observes on these curves that the self-focused propagation is favored when the laser is focused near the entrance of the gas jet. When focused in the middle of the gas jet (curve C), there is still a strong amplification of the maximum laser intensity compared to the vacuum case, but the laser seems to bounce back and almost no self-focusing occurs. We observed, however, that some part of the laser pulse has self-focused propagation between $z/z_R=2$ and 4 with $I/I_0 \approx 0.2$ and a rather large spot. The corresponding density wake is

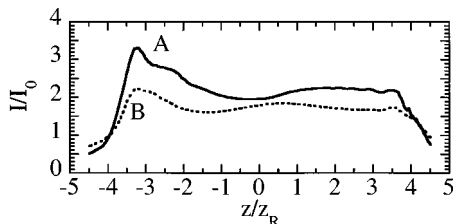


FIG. 8. On-axis maximum intensity for cylindrical (curve A) and slab (curve B) geometries. Parameters correspond to those of curves A of Fig. 7.

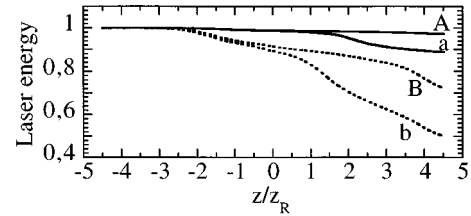


FIG. 9. Laser energy in the simulation box. Curves A and a correspond to the parameters of curve A of Fig. 7(b) (i.e., $n_0=3.5 \times 10^{18} \text{ cm}^{-3}$), and curves B and b correspond to the parameters of curve B of Fig. 7(b) (i.e., $n_0=7 \times 10^{18} \text{ cm}^{-3}$). The radius of the simulation box is $10r_L$ for curves a and b, and $20r_L$ for curves A and B.

still significant, since for $z/z_R=3.5$ the wake electron density oscillates between 0.6 and $1.5n_0$.

Figure 8 shows a comparison of cylindrical (curve A) and slab (curve B) geometry for the same set of numerical parameters. As expected, and already noticed by Pukhov and Meyer-ter-Vehn in a higher density case,²³ the cylindrical case leads to a higher on-axis intensity than the slab case. Similarly, we verified that the electron density cavitation was less important in the slab case. These effects have to be kept in mind while using slab results to interpret real experiments.

Figure 9 shows the laser energy in the simulation box normalized to its initial value versus the propagation distance for the parameters of Fig. 7(b) (i.e., $n_0=3.5 \times 10^{18} \text{ cm}^{-3}$ corresponding to curves a and A, and $n_0=7 \times 10^{18} \text{ cm}^{-3}$ corresponding to curves b and B). The radius of the simulation box is $10r_L$ for curves a and b, and $20r_L$ for curves A and B. The difference between the lower case and upper case curves is indicative of the fraction of laser energy side scattered out of the simulation region. At higher density there is a greater depletion of laser energy associated with creating the plasma wake.

V. CONCLUSION

We have derived the fast time averaged equations for the motion of particles and the generation of electromagnetic wake fields under the action of the ponderomotive potential of an ultraintense laser pulse propagating through a tenuous plasma. Based on these averaged equations, we have designed a new particle code calculating the particle trajectories on the plasma period time scale. This code is able to deal with cylindrically symmetric geometry as well as slab geometry. As an example of the use of the code we have studied stable propagation in the regime of total electron cavitation, with relativistic electrons ejected from the wake of the pulse in a cone whose angle decreases with energy. This calculation could also help in improving the interpretation of recent experiments on relativistic self-focusing.^{17,18}

As the code is based on a multiple time and space scale formulation of the governing equations its regime of validity is restricted to propagation of pulses in tenuous plasmas, $\omega_p \ll \omega_0$. However, it is this regime which is particularly difficult to treat with PIC codes. Additionally, the assumption has been made that the radiation is dominantly forward propagating, which eliminates the possibility of studying Raman backscattered waves with the present code. Also the

quasistatic approximation, in which it is assumed that the shape of the laser pulse changes only lightly in the time during which a given electron remains in the laser pulse, restricts from consideration those electrons which have been accelerated to high energy, $1 - v_z/c \gg \omega_p/\omega_0$. Finally, the code uses the predictor corrector method of calculation of the wake magnetic field. It has been our observation that for extremely intense and relatively long pulses that this can lead to some numerical difficulty.

One of the characteristics of the code is that it has a particularly low numerical noise. We have taken advantage of this to study the magnetic field generated in the wake of an ultra-intense field in a separate paper.²⁴ This magnetic field appears to be of fourth order in power of the laser field amplitude A and may play an important role in the laser wake field accelerator concept.

The code is presently devoted to the study of the interaction of laser pulses with plasmas. In many experiments however the laser pulse primarily interacts with a neutral gas, and the ionization processes may play an important role in the laser propagation itself.²⁵ We are currently incorporating an ionization package in the model to be able to deal with these aspects. The result will be a versatile and most efficient model to describe ultrashort pulse interaction with gas or preformed plasma.

ACKNOWLEDGMENT

The authors would like to thank C. McKinstrie for information regarding the derivation of the ponderomotive potential.

APPENDIX A: PONDEROMOTIVE EQUATIONS

In this appendix we derive the fast time averaged equations for the motion of particles in the laser pulse wake and the electromagnetic wake fields. We begin the derivation with the equations of motion for relativistic particles in electromagnetic fields described by a scalar and vector potential,

$$\frac{d}{dt} \left(\mathbf{p} + \frac{q}{c} \mathbf{A} \right) = -q \nabla \Phi + \left(\nabla \frac{q}{c} \mathbf{A} \right) \cdot \mathbf{v}, \quad (\text{A1})$$

where \mathbf{p} is the particle momentum, γ is the relativistic factor, $\mathbf{v} = \mathbf{p}/(\gamma m)$ is the particle velocity, and \mathbf{A} and Φ are the vector and scalar potentials. The total time derivative appearing in Eq. (A1) is the Lagrangian derivative following the particle velocity \mathbf{v} . Equation (A1) can be supplemented by the equation of evolution of particle energy,

$$\frac{d}{dt} \gamma m c^2 = -q \mathbf{v} \cdot \left(\nabla \Phi + \frac{1}{c} \frac{\partial \mathbf{A}}{\partial t} \right), \quad (\text{A2})$$

which will be useful in the following derivation.

The fields are determined by Maxwell's equations which are written as

$$\left[\frac{1}{c^2} \frac{\partial^2}{\partial t^2} - \nabla^2 \right] \mathbf{A} = \frac{4\pi}{c} \mathbf{j} - \nabla \left(\frac{1}{c} \frac{\partial \Phi}{\partial t} + \nabla \cdot \mathbf{A} \right), \quad (\text{A3})$$

$$\nabla \cdot \left[\nabla \Phi + \frac{1}{c} \frac{\partial \mathbf{A}}{\partial t} \right] = -4\pi \rho, \quad (\text{A4})$$

where \mathbf{j} and ρ are the current density and charge density, respectively. We calculate these by assuming that the plasma consists of an ensemble of cold fluids whose velocities are determined by Eqs. (A1) and (A2), and whose corresponding densities are determined by the continuity equation,

$$\frac{\partial n}{\partial t} + \nabla \cdot n \mathbf{v} = 0, \quad (\text{A5})$$

The charge and current densities are then obtained by averaging over the ensemble of cold fluids $\rho = \langle qn \rangle$ and $\mathbf{j} = \langle qn \mathbf{v} \rangle$. This averaging will be performed after the averaging over the fast time scale of the radiation. Further, we temporarily specialize to the Coulomb gauge where $\nabla \cdot \mathbf{A} = 0$.

The next step is to transform to laser frame coordinates by introducing the variable $\zeta = z - ct$. In terms of this new axial coordinate Eqs. (A1) and (A2) can be written as

$$\left[\frac{\partial}{\partial t} + (\mathbf{v} - c \mathbf{e}_z) \cdot \nabla \right] \left(\mathbf{p} + \frac{q}{c} \mathbf{A} \right) = -q \nabla \Phi + \left(\nabla \frac{q}{c} \mathbf{A} \right) \cdot \mathbf{v}, \quad (\text{A6})$$

$$\left[\frac{\partial}{\partial t} + (\mathbf{v} - c \mathbf{e}_z) \cdot \nabla \right] \gamma m c^2 = -q \mathbf{v} \cdot \left(\nabla \Phi + \frac{1}{c} \frac{\partial \mathbf{A}}{\partial t} - \frac{\partial \mathbf{A}}{\partial \zeta} \right). \quad (\text{A7})$$

Here, the axial component of the gradient operator is understood to represent differentiation with respect to ζ . Further, Maxwell's equations in the Coulomb gauge become,

$$\left[\frac{1}{c^2} \frac{\partial^2}{\partial t^2} - \frac{2}{c} \frac{\partial^2}{\partial t \partial \zeta} - \nabla_{\perp}^2 \right] \mathbf{A} = \frac{4\pi}{c} \mathbf{j} - \nabla \left(\frac{1}{c} \frac{\partial \Phi}{\partial t} - \frac{\partial \Phi}{\partial \zeta} \right), \quad (\text{A8})$$

and,

$$\nabla_{\perp}^2 \Phi + \frac{\partial^2}{\partial \zeta^2} \Phi = -4\pi \rho. \quad (\text{A9})$$

Rather than solving the three independent components of Eq. (A6), we consider our system to be the two components of Eq. (A6) transverse to the direction of propagation of the laser pulse,

$$\begin{aligned} & \left[\frac{\partial}{\partial t} + (\mathbf{v} - c \mathbf{e}_z) \cdot \nabla \right] \left(\mathbf{p}_{\perp} + \frac{q}{c} \mathbf{A}_{\perp} \right) \\ & = -q \nabla_{\perp} \Phi + \left(\nabla_{\perp} \frac{q}{c} \mathbf{A} \right) \cdot \mathbf{v}, \end{aligned} \quad (\text{A10})$$

and the axial component of Eq. (A6) minus Eq. (A7) divided by the speed of light,

$$\begin{aligned} & \left[\frac{\partial}{\partial t} + (\mathbf{v} - c \mathbf{e}_z) \cdot \nabla \right] \left[p_z - \gamma m c + \frac{q}{c} (A_z - \Phi) \right] \\ & = -\frac{q}{c} \left(\frac{\partial \Phi}{\partial t} - \frac{\mathbf{v}}{c} \cdot \frac{\partial \mathbf{A}}{\partial t} \right), \end{aligned} \quad (\text{A11})$$

The next step in our derivation is to introduce an expansion based on the disparity between the laser and plasma frequencies. We define the small parameter $\epsilon = \omega_p/\omega_0$ where ω_p is the plasma frequency and ω_0 is the laser frequency. In terms of this small parameter the axial, L , and transverse, R ,

sizes of the laser pulse scale as $R \approx L \approx \lambda_0/\epsilon$, where λ_0 is the laser wavelength. Derivatives with respect to the axial variable ζ are expanded as follows:

$$\frac{\partial}{\partial \zeta} = \frac{\partial}{\partial \zeta_0} + \frac{\partial}{\partial \zeta_1}, \quad (A12)$$

where ζ_0 is a fast variable associated with the laser wavelength $\partial/\partial \zeta_0 \approx 1/\lambda_0$, and ζ_1 is a slow variable associated with the laser envelope and the plasma wavelength, $\partial/\partial \zeta_1 \approx \epsilon/\lambda_0$. The transverse gradient is also assumed to follow the scaling, $\nabla_{\perp} \approx \epsilon/\lambda_0$. In the laser frame coordinates all quantities vary slowly in time. Correspondingly, we take the time derivative to scale as $\partial/\partial t \approx \epsilon^2 \omega_0$. Next we expand the field quantities Φ and \mathbf{A} in powers of ϵ . As it turns out, only the lowest order terms in each field quantity enter the final equations. Thus, we suppress the subscript, 0, for the lowest order quantities but retain it when expressing the higher order quantities. For situations of interest the particle motion is relativistic. Thus, it is appropriate to consider the magnitude of the lowest order quantities Φ and \mathbf{A} to scale as mc^2/q . Consequently, the source terms involving ρ and \mathbf{j} in Eqs. (A8) and (A9) are second-order quantities scaling as $\epsilon^2 = (\omega_p/\omega_0)^2$.

The leading (zero) order version of the Poisson equation, $\partial^2 \Phi / \partial \zeta_0^2 = 0$, requires that the lowest order electrostatic potential be independent of the fast variable ζ_0 , $\Phi = \bar{\Phi}(\zeta_1, \mathbf{x}_{\perp}, t)$. Here the overbar indicates that a quantity is averaged over the fast space scale. Similarly, the lowest order version of the gauge condition, $\partial A_z / \partial \zeta_0 = 0$, requires that the zero-order axial component of the vector potential be independent of the fast variable ζ_0 , $A_z = \bar{A}_z(\zeta_1, \mathbf{x}_{\perp}, t)$. This follows from the fact that the transverse gradient is assumed to be first order. Together these conditions require that the zero-order axial electric field vanish. The first-order version of the Poisson equation, $\partial^2 \Phi_1 / \partial \zeta_0^2 + 2\partial^2 \Phi / \partial \zeta_0 \partial \zeta_1 = 0$, then indicates that the first-order potential, Φ_1 is also independent of the fast variable [Note that in the above the second term is identically zero as a result of the lowest order solution, $\Phi = \bar{\Phi}(\zeta_1, \mathbf{x}_{\perp}, t)$.] Finally, in second order the charge density enters,

$$\nabla_{\perp}^2 \bar{\Phi} + \frac{\partial^2}{\partial \zeta_1^2} \bar{\Phi} + \frac{\partial^2}{\partial \zeta_0^2} \Phi_2 = -4\pi\rho.$$

Averaging this equation over the fast scale annihilates the second-order potential and indicates that only the average charge density contributes to the lowest order potential. The averaging step will be performed later in the derivation, once the charge density is determined. The rapidly varying part of the charge density produces a second-order contribution to the electrostatic potential. The physical implication of the above equations is that in tenuous plasmas large electrostatic potentials can only develop over distances much greater than the laser wavelength.

The lowest (zero)-order contribution to the transverse component of the vector potential has both a rapidly varying component and an averaged component,

$$\mathbf{A}_{\perp} = \tilde{\mathbf{A}}_{\perp}(\zeta_0, \zeta_1, \mathbf{x}_{\perp}, t) + \bar{\mathbf{A}}_{\perp}(\zeta_1, \mathbf{x}_{\perp}, t). \quad (A13)$$

The rapidly varying component is associated with the laser field, and the slowly varying component is associated with the electromagnetic component of the wake. Both compo-

nents are determined by the leading order version of Eq. (A8) which is second order in ϵ . We note that the transverse components of Eq. (A8) are second order. Thus the average of (A8) will determine the electromagnetic field of the wake, while the rapidly varying part describes the propagation of the laser light. Solution of this equation will also be deferred until the charge and current densities are determined.

We now consider solution of the particle equations. Within the approximation that quantities evolve slowly in the laser frame we may neglect the time derivatives in Eq. (A11) through two orders in ϵ . Further assuming that the particle velocity satisfies the condition $1 - v_z/c \gg \epsilon$, Eq. (A11) yields

$$\gamma mc - p_z = mc + \frac{q}{c} (\bar{A}_z - \bar{\Phi}), \quad (A14)$$

where we have inserted overbars on the potential Φ and A_z indicating that they do not vary on the scale of the laser wavelength. Equation (A14) indicates the constancy of the quantity $H - cP_z$, where H is the particle Hamiltonian and P_z the canonical momentum, for cases in which the fields depend on time only in the combination $z - ct$. The value of this conserved quantity is determined from the condition that the plasma electrons be unperturbed upstream from the laser pulse. It is important to note that Eq. (A14) indicates that, while the quantities γ and p_z have both rapidly and slowly varying components, their difference is a slowly varying quantity. The condition $1 - v_z/c \gg \epsilon$ requires that one wavelength of the laser field pass by electrons in a time sufficiently short such that their radial motion is negligible. This condition (which will appear again) effectively excludes from consideration the motion of electrons which have been trapped and accelerated to high energy by the laser pulse.

Turning now to the transverse components of the momentum, the lowest order version of (A10) gives $\partial(\mathbf{p}_{\perp} + q\mathbf{A}_{\perp}/c)/\partial \zeta_0 = 0$. Thus,

$$\mathbf{p}_{\perp} = \tilde{\mathbf{p}}_{\perp}(\zeta_0, \zeta_1, \mathbf{x}_{\perp}, t) + \bar{\mathbf{p}}_{\perp}(\zeta_1, \mathbf{x}_{\perp}, t) \quad (A15)$$

where

$$\tilde{\mathbf{p}}_{\perp}(\zeta_0, \zeta_1, \mathbf{x}_{\perp}, t) = -\frac{q}{c} \tilde{\mathbf{A}}_{\perp}(\zeta_0, \zeta_1, \mathbf{x}_{\perp}, t), \quad (A16)$$

is the lowest (zero)-order transverse jitter momentum associated with the laser field. We note that there is also a zeroth-order longitudinal component of the jitter momentum which can be calculated from Eq. (A14) once the rapidly varying component of the kinetic energy is determined. The averaged transverse momentum (also zero order) is determined from the first-order version of Eq. (A10)

$$\left[\mathbf{p}_{\perp} \cdot \nabla_{\perp} + (\bar{p}_z - \bar{\gamma}mc) \frac{\partial}{\partial \zeta_1} \right] \left(\bar{\mathbf{p}}_{\perp} + \frac{q}{c} \bar{\mathbf{A}}_{\perp} \right) + (\bar{p}_z - \bar{\gamma}mc) \times \frac{\partial}{\partial \zeta_0} \left(\mathbf{p}_{\perp 1} + \frac{q}{c} \mathbf{A}_{\perp 1} \right) = -q\gamma m \nabla_{\perp} \bar{\Phi} + \left(\nabla_{\perp} \frac{q}{c} \mathbf{A} \right) \cdot \mathbf{p}. \quad (A17)$$

Here we have multiplied by γm , and used Eq. (A14) to replace $p_z - \gamma mc$ by its average. We have also indicated the necessary presence of first-order corrections to the transverse

momentum and vector potential. These however, are annihilated by averaging Eq. (A17) over the fast length scale,

$$\begin{aligned} & \left[\bar{\mathbf{p}}_{\perp} \cdot \nabla_{\perp} + (\bar{p}_z - \bar{\gamma}mc) \frac{\partial}{\partial \zeta_1} \right] \left(\bar{\mathbf{p}}_{\perp} + \frac{q}{c} \bar{\mathbf{A}}_{\perp} \right) \\ &= -q \bar{\gamma}m \nabla_{\perp} \bar{\Phi} + \overline{\left(\nabla_{\perp} \frac{q}{c} \bar{\mathbf{A}} \right) \cdot \mathbf{p}} \end{aligned} \quad (\text{A18})$$

Thus, except for the last term on the right-hand side, all the quantities appearing in Eq. (A18) are averaged quantities. The last term on the right is evaluated as follows:

$$\overline{\left(\nabla_{\perp} \frac{q}{c} \bar{\mathbf{A}} \right) \cdot \mathbf{p}} = \left(\nabla_{\perp} \frac{q}{c} \bar{\mathbf{A}} \right) \cdot \bar{\mathbf{p}} - \frac{1}{2} \nabla_{\perp} \overline{\left| \frac{q}{c} \tilde{\mathbf{A}}_{\perp} \right|^2}, \quad (\text{A19})$$

where we have used Eq. (A16) to express the rapidly varying momentum, and we have used the fact that the axial vector potential has only a slowly varying component.

We now derive an expression for the fast scale averaged relativistic factor. We begin by writing an expression for the square of the zero-order relativistic factor,

$$\gamma^2 = 1 + \frac{1}{m^2 c^2} \left[\left| \bar{\mathbf{p}}_{\perp} - \frac{q}{c} \tilde{\mathbf{A}}_{\perp} \right|^2 + p_z^2 \right], \quad (\text{A20})$$

where we have expressed the rapidly varying part of the perpendicular momentum in terms of the vector potential. We then use Eq. (A14) to express the axial momentum in terms of its average and the relativistic factor, $p_z = \bar{p}_z + mc(\gamma - \bar{\gamma})$. Inserting this expression in Eq. (A20) and averaging over the fast time scale produces,

$$\bar{\gamma}^2 = 1 + \frac{1}{m^2 c^2} \left[\overline{|\bar{\mathbf{p}}_{\perp}|^2} + \bar{p}_z^2 + \overline{\left| \frac{q}{c} \tilde{\mathbf{A}}_{\perp} \right|^2} \right], \quad (\text{A21})$$

Thus, the average relativistic factor depends algebraically on the average momentum, and radiation vector potential in a straightforward way.

We then introduce the fast scale averaged velocity which we define via the relation,

$$\bar{\mathbf{v}} \equiv \frac{\bar{\mathbf{p}}}{\bar{\gamma}m} \quad (\text{A22})$$

With this definition, Eqs. (A18), (A19), and (A20) may be combined and rewritten,

$$\begin{aligned} & (\bar{\mathbf{v}} - \mathbf{e}_z c) \cdot \nabla \left(\bar{\mathbf{p}}_{\perp} + \frac{q}{c} \bar{\mathbf{A}}_{\perp} \right) \\ &= -q \nabla_{\perp} \bar{\Phi} + \left(\nabla_{\perp} \frac{q}{c} \bar{\mathbf{A}} \right) \cdot \bar{\mathbf{v}} - \frac{1}{2m\bar{\gamma}} \nabla_{\perp} \overline{\left| \frac{q}{c} \tilde{\mathbf{A}}_{\perp} \right|^2} \end{aligned} \quad (\text{A23})$$

Thus, we recover an averaged equation of motion which is of the same form as the original equation for the unaveraged quantities, (A10), except that time derivatives are absent (replaced by a derivative with respect to z in the quasistatic approximation), and there is a ponderomotive potential due to the jitter of electrons in the laser field.

Equation (A23) describes the evolution of the perpendicular components of momentum. The evolution equation for the parallel component of momentum can be obtained by

combining Eq. (A23), the definition of the average relativistic factor Eq. (A21), and the constant of motion, Eq. (A14). The result, after considerable algebra, is

$$\begin{aligned} & (\bar{\mathbf{v}} - \mathbf{e}_z c) \cdot \nabla \left(\bar{p}_z + \frac{q}{c} \bar{A}_z \right) \\ &= -q \frac{\partial \bar{\Phi}}{\partial \zeta} + \left(\frac{\partial}{\partial \zeta} \frac{q}{c} \bar{\mathbf{A}} \right) \cdot \bar{\mathbf{v}} - \frac{1}{2m\bar{\gamma}} \frac{\partial}{\partial \zeta} \overline{\left| \frac{q}{c} \tilde{\mathbf{A}}_{\perp} \right|^2}, \end{aligned} \quad (\text{A24})$$

which is again of the same form as the original, unaveraged equation of motion, (A10). Combining Eqs. (A23) and (A24) one can write all components of the equation of motion in the following form:

$$(\bar{\mathbf{v}} - \mathbf{e}_z c) \cdot \nabla \bar{\mathbf{p}} = q \left(\bar{\mathbf{E}} + \frac{\bar{\mathbf{v}} \times \bar{\mathbf{B}}}{c} \right) - \frac{1}{2m\bar{\gamma}} \nabla \overline{\left| \frac{q}{c} \tilde{\mathbf{A}}_{\perp} \right|^2}, \quad (\text{A25})$$

where \bar{E} and \bar{B} are the wake electric and magnetic fields. Finally, using Eqs. (A21), (A23), and (A24) the evolution of the averaged particle energy is determined by

$$\begin{aligned} & (\bar{\mathbf{v}} - \mathbf{e}_z c) \cdot \nabla \bar{\gamma} m c^2 \\ &= -q \bar{\mathbf{v}} \cdot \left(\nabla \bar{\Phi} - \frac{\partial \bar{\mathbf{A}}}{\partial \zeta} \right) - \frac{c}{2m\bar{\gamma}} \frac{\partial}{\partial \zeta} \overline{\left| \frac{q}{c} \tilde{\mathbf{A}}_{\perp} \right|^2} \end{aligned} \quad (\text{A26})$$

We now focus on the field equations for which we must calculate the charge and current densities. The charge density for each cold fluid in the ensemble is obtained from the particle density which satisfies the continuity equation, (A5). Written in laser coordinates Eq. (A5) appears as

$$\nabla_{\perp} \cdot \mathbf{p}_{\perp} \frac{n}{\gamma} + \left[\frac{\partial}{\partial \zeta_0} + \frac{\partial}{\partial \zeta_1} \right] (p_z - \gamma mc) \frac{n}{\gamma} = 0, \quad (\text{A27})$$

where we have multiplied through by the mass to express the velocities in terms of momenta. The lowest order version of Eq. (A27),

$$\frac{\partial}{\partial \zeta_0} (p_z - \gamma mc) \frac{n}{\gamma} = 0,$$

requires that the ratio n/γ be a slowly varying quantity, $n/\gamma = \bar{n}/\bar{\gamma}$. Here we have used the fact that the lowest order version of $p_z - \gamma mc$ is a slowly varying quantity, $p_z - \gamma mc = \bar{p}_z - \bar{\gamma}mc$. In first order Eq. (A27) becomes

$$\begin{aligned} & \nabla_{\perp} \cdot \mathbf{p}_{\perp} \left(\frac{\bar{n}}{\bar{\gamma}} \right) + \frac{\partial}{\partial \zeta_1} (\bar{p}_z - \bar{\gamma}mc) \left(\frac{\bar{n}}{\bar{\gamma}} \right) \\ &+ \frac{\partial}{\partial \zeta_0} \left[(p_z - \gamma mc) \frac{n}{\gamma} \right] = 0, \end{aligned}$$

where we have indicated the necessary presence of first-order corrections to the density, axial momentum, and relativistic factor. As before these corrections are annihilated on averaging over the fast length scale,

$$\nabla_{\perp} \cdot \bar{\mathbf{p}}_{\perp} \left(\frac{\bar{n}}{\bar{\gamma}} \right) + \frac{\partial}{\partial \zeta_1} (\bar{p}_z - \bar{\gamma}mc) \left(\frac{\bar{n}}{\bar{\gamma}} \right) = 0, \quad (\text{A28})$$

Given the ratio n/γ is a slowly varying quantity, we conclude

$$\bar{n} = \overline{\gamma \left(\frac{n}{\gamma} \right)}. \quad (\text{A29})$$

Introducing the velocity defined in Eq. (A22) we observe that the average quantities also obey the continuity equation,

$$\nabla_{\perp} \cdot \mathbf{v}_{\perp} \bar{n} + \frac{\partial}{\partial \zeta_1} (\bar{v}_z - c) \bar{n} = 0. \quad (\text{A30})$$

The space and ensemble averaged density is then inserted in the space averaged Poisson equation,

$$\nabla_{\perp}^2 \bar{\Phi} + \frac{\partial^2}{\partial \zeta_1^2} \bar{\Phi} = -4\pi q \langle \bar{n} \rangle. \quad (\text{A31})$$

Included in the density is the contribution of both electrons and ions.

Finally, we need to calculate current density to be inserted in Eq. (A8). We separate this equation into its rapidly varying component,

$$\left[\frac{2}{c} \frac{\partial^2}{\partial t \partial \zeta_0} + \nabla_{\perp}^2 \right] \tilde{\mathbf{A}}_{\perp} = -\frac{4\pi}{c} \tilde{\mathbf{j}}_{\perp}, \quad (\text{A32})$$

and its slowly varying component,

$$\nabla_{\perp}^2 \bar{\mathbf{A}} = -\frac{4\pi}{c} \bar{\mathbf{j}} - \nabla \left(\frac{\partial \bar{\Phi}}{\partial \zeta_1} \right). \quad (\text{A33})$$

The rapidly varying component of the current density can then be expressed in terms of the laser vector potential and the average density and relativistic factor,

$$\tilde{\mathbf{j}}_{\perp} = \frac{q}{m} \left\langle \left(\frac{n}{\gamma} \right) \tilde{\mathbf{p}}_{\perp} \right\rangle = -\frac{q^2}{mc} \left\langle \frac{\bar{n}}{\bar{\gamma}} \right\rangle \tilde{\mathbf{A}}_{\perp}, \quad (\text{A34})$$

where we have used Eq. (A29). Similarly, the average current can be written as

$$\bar{\mathbf{j}} = \frac{q}{m} \left\langle \left(\frac{n}{\gamma} \right) \bar{\mathbf{p}} \right\rangle = q \langle \bar{n} \bar{\mathbf{v}} \rangle. \quad (\text{A35})$$

The final system of averaged equations consists of Eqs. (A14), (A21)–(A23), and (A30)–(A35). It is interesting to note that the averaged quantities obey essentially the same equations as the unaveraged quantities except for the addition of the ponderomotive force in Eq. (A25) and the revised definition of the relativistic factor (A21). Thus, in solving these equations, the only quantity that needs to be averaged over the fast space scale is the square of the laser vector potential appearing in Eq. (A21). All the other averaged quantities are derived from this. The additional ensemble averaging of cold fluids may be done either by solving for the evolution of an ensemble of particles (as done in this paper) and computing the charge and current densities on a grid, or by introducing a distribution function and the appropriate kinetic equation. We note that the restriction to the Coulomb gauge can easily be lifted by comparing the averaged equations to the unaveraged ones. The results are that Eqs. (A31) and (A33) are replaced by the following:

$$\nabla^2 \bar{\Phi} - \frac{\partial}{\partial \zeta_1} \nabla \cdot \bar{\mathbf{A}} = -4\pi q \langle \bar{n} \rangle, \quad (\text{A36})$$

and

$$\nabla_{\perp}^2 \bar{\mathbf{A}} = -\frac{4\pi}{c} \bar{\mathbf{j}} - \nabla \left(\frac{\partial \bar{\Phi}}{\partial \zeta_1} - \nabla \cdot \bar{\mathbf{A}} \right), \quad (\text{A37})$$

respectively.

As a final comment we note that the expression for the ponderomotive force in Eq. (A26) has been derived a number of times in the literature previously. In particular, for the case of circular polarization this result is equivalent to that published in Refs. 26 and 27. In the case of elliptically or linearly polarized radiation there is an inconsistency between our result and those of Ref. 26. However, our results are consistent with earlier derivations,^{28,29} using different approaches to the equations of motion. Further, our results are consistent in the fluid limit with those published in Ref. 2. The various discrepancies, which are only noticeable when the jitter motion is relativistic, seem to be related to the correct inclusion of the high frequency component of the axial momentum. In particular, the presence of this component of the momentum allows the particularly simple Eq. (A21) to be derived from Eq. (A20).

APPENDIX B: CONSERVATION LAWS

In this appendix we derive two conservation laws for our system of ponderomotive equations; the conservation of laser wave action, and the conservation of particle and field energy. Our derivations follow closely those presented in Ref. 8. We begin by writing the radiation field in terms of a rapidly varying phase and an envelope,

$$\tilde{\mathbf{A}}_{\perp} = \hat{\mathbf{A}}_{\perp} \exp[ik_0 \zeta_0] + \text{c.c.} \quad (\text{B1})$$

The evolution of the envelope is then determined by substituting Eq. (B1) in Eq. (A32),

$$\left[\frac{2}{c} \frac{\partial}{\partial t} \left(ik_0 + \frac{\partial}{\partial \zeta} \right) + \nabla_{\perp}^2 \right] \hat{\mathbf{A}}_{\perp} = \frac{4\pi q^2}{mc^2} \left\langle \frac{\bar{n}}{\bar{\gamma}} \right\rangle \hat{\mathbf{A}}_{\perp}. \quad (\text{B2})$$

The para-axial approximation consists of neglecting the ζ derivative in comparison with the lowest order wave number k_0 . As the plasma density becomes modulated the phase of the laser envelope will develop increasingly rapid variations with axial distance, at some point the z derivative will no longer be negligible. Thus, we will keep this term here as it becomes important with time as the laser field decays and the laser frequency drops. To derive the conservation of wave action we multiply Eq. (B2) by $\hat{\mathbf{A}}_{\perp}^*$, integrate over all volume, and subtract from that quantity its complex conjugate,

$$\begin{aligned} & \frac{d}{dt} 2ik_0 \int d^3x |\hat{\mathbf{A}}_{\perp}|^2 \\ & + 2 \int d^3x \left[\hat{\mathbf{A}}_{\perp}^* \cdot \frac{\partial^2}{\partial t \partial \zeta} \hat{\mathbf{A}}_{\perp} - \hat{\mathbf{A}}_{\perp} \cdot \frac{\partial^2}{\partial t \partial \zeta} \hat{\mathbf{A}}_{\perp}^* \right] = 0. \end{aligned} \quad (\text{B3})$$

Here we have assumed the laser amplitude vanishes at infinity so that boundary terms can be neglected. We now use the identity,

$$\int d^3x \left[\hat{\mathbf{A}}_{\perp}^* \cdot \frac{\partial^2}{\partial t \partial \zeta} \hat{\mathbf{A}}_{\perp} - \hat{\mathbf{A}}_{\perp} \cdot \frac{\partial^2}{\partial t \partial \zeta} \hat{\mathbf{A}}_{\perp}^* \right] \\ = \frac{1}{2} \frac{\partial}{\partial t} \int d^3x \left[\hat{\mathbf{A}}_{\perp}^* \cdot \frac{\partial}{\partial \zeta} \hat{\mathbf{A}}_{\perp} - \hat{\mathbf{A}}_{\perp} \cdot \frac{\partial}{\partial \zeta} \hat{\mathbf{A}}_{\perp}^* \right],$$

to rewrite Eq. (B3) as a conservation law,

$$\frac{d}{dt} \left\{ 2ik_0 \int d^3x |\tilde{\mathbf{A}}_{\perp}|^2 \right. \\ \left. + \int d^3x \left[\hat{\mathbf{A}}_{\perp}^* \cdot \frac{\partial}{\partial \zeta} \hat{\mathbf{A}}_{\perp} - \hat{\mathbf{A}}_{\perp} \cdot \frac{\partial}{\partial \zeta} \hat{\mathbf{A}}_{\perp}^* \right] \right\} = 0. \quad (B4)$$

The interpretation of the above as conservation of action follows from the identification of the second term as the shift in wave number from the reference value k_0 . Thus, Eq. (B4) can be viewed as the integral of the product of the local wave number multiplied by the square of the vector potential. Given that wave number and frequency are linearly related in a low density plasma this corresponds to the action.

To obtain a conservation of energy relation, we form the energy associated with the laser pulse,

$$U_L = \frac{1}{2\pi} \int d^3x \left[ik_0 \hat{\mathbf{A}}_{\perp} + \frac{\partial \hat{\mathbf{A}}_{\perp}}{\partial \zeta} \right]^2, \quad (B5)$$

which represents the sum of the electric and magnetic energy of the pulse. Differentiation of this quantity with respect to time, and use of Eq. (B2) and its conjugate give,

$$\frac{dU_L}{dt} = \frac{c}{4\pi} \int d^3x \frac{4\pi q^2}{mc^2} \left\langle \frac{\bar{n}}{\bar{\gamma}} \right\rangle \frac{\partial}{\partial \zeta} |\hat{\mathbf{A}}_{\perp}|^2, \quad (B6)$$

where we have assumed that the radiation field vanishes at the boundary of the volume in carrying out a number of integrations by parts.

The evolution of the particle energy is determined by multiplying Eq. (A26) for each member of the ensemble of fluids by its corresponding density, \bar{n} , and averaging over the ensemble,

$$\nabla \cdot \langle (\bar{\mathbf{v}} - \mathbf{e}_z c) \bar{n} \bar{\gamma} \rangle mc^2 \\ = -\bar{\mathbf{j}} \cdot \left(\nabla \bar{\Phi} - \frac{\partial \bar{\mathbf{A}}}{\partial \zeta} \right) - \frac{c}{2m} \left\langle \frac{\bar{n}}{\bar{\gamma}} \right\rangle \frac{\partial}{\partial \zeta} \left| \frac{q}{c} \tilde{\mathbf{A}}_{\perp} \right|^2, \quad (B7)$$

where the plasma wake current density is given by Eq. (A35). Using Eq. (A33), integrating over the simulation volume, and noting cancellations we have

$$\int d^3x \nabla \cdot \langle (\bar{\mathbf{v}} - \mathbf{e}_z c) \bar{n} \bar{\gamma} \rangle mc^2 \\ = \int d^3x \frac{c}{8\pi} \frac{\partial}{\partial \zeta} [|\nabla(\bar{\Phi} - \bar{A}_z)|^2 + |\nabla_{\perp} \times \bar{\mathbf{A}}_{\perp}|^2] \\ - \int d^3x \frac{c}{2m} \left\langle \frac{\bar{n}}{\bar{\gamma}} \right\rangle \frac{\partial}{\partial \zeta} \left| \frac{q}{c} \tilde{\mathbf{A}}_{\perp} \right|^2. \quad (B8)$$

Replacing the last term in Eq. (B8) using Eqs. (B1) and (B6), and noting that the contributions from the remaining two terms can be expressed in terms of surface integrals up- and downstream from the laser pulse we obtain,

$$\frac{dU_L}{dt} = \int d^2x_{\perp} \left\{ \frac{c}{8\pi} [|\nabla(\bar{\Phi} - \bar{A}_z)|^2 + |\nabla_{\perp} \times \bar{\mathbf{A}}_{\perp}|^2] \right. \\ \left. + \langle (c - \bar{v}_z) \bar{n} \bar{\gamma} \rangle mc^2 \right\}_{z=-\infty}^{z=\infty}. \quad (B9)$$

Here, $z=\infty$ represents a surface upstream from the pulse where the plasma is undisturbed, and $z=-\infty$ is a surface downstream from the pulse across which the plasma wake passes. Thus, Eq. (B9) shows that energy extracted from the laser pulse is used to accelerate plasma electrons and to create the wake electric and magnetic fields.

- ¹T. M. Antonsen, Jr. and P. Mora, Phys. Rev. Lett. **69**, 2204 (1992); Phys. Fluids B **5**, 1440 (1993).
- ²P. Sprangle, E. Esarey, J. Krall, and G. Joyce, Phys. Rev. Lett. **69**, 2200 (1992); J. Krall, A. Ting, E. Esarey, and P. Sprangle, Phys. Rev. E **48**, 2157 (1993).
- ³N. E. Andreev, L. M. Gorbunov, V. I. Kirsanov, A. A. Pogosova, and R. R. Ramazashvili, JETP Lett. **55**, 571 (1992).
- ⁴X. L. Chen and R. N. Sudan, Phys. Fluids B **5**, 1336 (1993).
- ⁵C. J. McKinstrie and R. Bingham, Phys. Fluids B **4**, 2626 (1992).
- ⁶W. B. Mori, C. D. Decker, D. E. Hinkel, and T. Katsouleas, Phys. Rev. Lett. **72**, 1482 (1994).
- ⁷C. D. Decker, W. B. Mori, and T. Katsouleas, Phys. Rev. E **50**, R3338 (1994); C. A. Coverdale, C. B. Darrow, C. D. Decker, W. B. Mori, K.-C. Tzeng, K. A. Marsh, C. E. Clayton, and C. Joshi, Phys. Rev. Lett. **74**, 4659 (1995); C. D. Decker, W. B. Mori, K.-C. Tzeng, and T. Katsouleas, Phys. Plasmas **3**, 2047 (1996).
- ⁸S. V. Bulanov, I. N. Inovenko, V. I. Kirsanov, N. M. Naumova, and A. S. Sakharov, Phys. Fluids B **4**, 1935 (1992); S. V. Bulanov, F. Pegoraro, and A. M. Pukhov, Phys. Rev. Lett. **74**, 710 (1995).
- ⁹G. Shvets and J. S. Wurtele, Phys. Rev. Lett. **73**, 3540 (1994).
- ¹⁰P. Sprangle, J. Krall, and E. Esarey, Phys. Rev. Lett. **73**, 3544 (1994).
- ¹¹C. G. Durfee III and H. M. Milchberg, Phys. Rev. Lett. **71**, 2409 (1993); C. G. Durfee III, J. Lynch, and H. M. Milchberg, Opt. Lett. **19**, 1937 (1994).
- ¹²P. Mora and T. M. Antonsen, Jr., Phys. Rev. E **53**, R2068 (1996).
- ¹³P. Sprangle, E. Esarey, and A. Ting, Phys. Rev. Lett. **64**, 2011 (1990).
- ¹⁴C. B. Darrow, C. Coverdale, M. D. Perry, W. B. Mori, C. Clayton, K. Marsh, and C. Joshi, Phys. Rev. Lett. **69**, 442 (1992); A. S. Sakharov and V. I. Kirsanov, Phys. Rev. E **49**, 3274 (1994); N. E. Andreev, V. I. Kirsanov, and L. M. Gorbunov, Phys. Plasmas **2**, 2573 (1995); Ph. Mounaix and D. Pesme, *ibid.* **1**, 2579 (1994); C. Rousseaux, G. Malka, J. L. Miquel, F. Amiranoff, S. D. Baton, and Ph. Mounaix, Phys. Rev. Lett. **74**, 4655 (1995).
- ¹⁵G. Schmidt and W. Horton, Comments Plasma Phys. Controlled Fusion **9**, 85 (1985); A. V. Litvak, Zh. Eksp. Teor. Fiz. **57**, 629 (1969) [Sov. Phys. JETP **30**, 344 (1969)]; P. Kaw, G. Schmidt, and T. Wilcox, Phys. Fluids **16**, 1522 (1973); C. E. Max, J. Arons, and A. B. Langdon, Phys. Rev. Lett. **33**, 209 (1974); X. L. Chen and R. N. Sudan, *ibid.* **70**, 2082 (1993).
- ¹⁶G. Z. Sun, E. Ott, Y. C. Lee, and P. Guzdar, Phys. Fluids **30**, 526 (1987).
- ¹⁷A. B. Borisov, A. V. Borovskiy, V. V. Korobkin, A. M. Prokhorov, O. B. Shiryayev, X. M. Shi, T. S. Luk, A. McPherson, J. C. Solem, K. Boyer, and C. K. Rhodes, Phys. Rev. Lett. **68**, 2309 (1992).
- ¹⁸P. Monot, T. Auguste, P. Gibbon, F. Jakober, G. Mainfray, A. Dulieu, M. Louis-Jacquet, G. Malka, and J. L. Miquel, Phys. Rev. Lett. **74**, 2953 (1995); P. Gibbon, P. Monot, T. Auguste, and G. Mainfray, Phys. Plasmas **2**, 1305 (1995); A. Chiron, G. Bonnaud, A. Dulieu, J. L. Miquel, G. Malka, M. Louis-Jacquet, and G. Mainfray, *ibid.* **3**, 1373 (1996).
- ¹⁹J. B. Rosenzweig, B. Breizman, T. Katsouleas, and J. J. Su, Phys. Rev. A **44**, R6189 (1991).
- ²⁰T. M. Antonsen, Jr. and P. Mora, Phys. Rev. Lett. **74**, 4440 (1995).
- ²¹D. W. Forslund, J. M. Kindel, W. B. Mori, C. Joshi, and J. M. Dawson, Phys. Rev. Lett. **54**, 558 (1985); L. D. Landau and E. M. Lifshitz, *Classical Theory of Fields*, 3rd ed. (Addison-Wesley, Reading, MA, 1971).
- ²²D. D. Meyerhofer, C. I. Moore, and J. P. Knauer, in *High Field Interactions and Short Wavelength Generation*, 1994 OSA Technical Digest Series (Optical Society of America, Washington, DC, 1994), Vol. 16, p. 121.
- ²³A. Pukhov and J. Meyer-ter-Vehn, Phys. Rev. Lett. **76**, 3975 (1996).

²⁴L. Gorbunov, P. Mora, and T. M. Antonsen, Jr., Phys. Rev. Lett. **76**, 2495 (1996).
²⁵T. Auguste, P. Monot, L.-A. Lompré, G. Mainfray, and C. Manus, Opt. Commun. **89**, 145 (1993); S. C. Rae, *ibid.* **97**, 25 (1993).

²⁶E. L. Lindman and M. A. Stroschio, Nucl. Fusion **17**, 619 (1977).
²⁷C. J. McKinstrie and D. F. Dubois, Phys. Fluids **31**, 278 (1988).
²⁸T. W. B. Kibble, Phys. Rev. **150**, 1060 (1966).
²⁹G. Schmidt and T. Wilcox, Phys. Rev. Lett. **31**, 1380 (1973).